NATO OTAN NURC

a NATO Research Centre
un Centre de Recherche de l'OTAN

NURC
PARTNERING FOR MARITIME INNOVATION

Reprint Series **NURC-PR-2008-007**

Tank measurements of scattering from a resin-filled fiberglass spherical shell with internal flaws

Alessandra Tesei, Piero Guerrini, Mario Zampolli

September 2008

Originally published in:

Journal of the Acoustical Society of America, Vol. 124, No. 2, August 2008, pp. 827-840.

About NURC

Our vision

- To conduct maritime research and develop products in support of NATO's maritime operational and transformational requirements.
- To be the first port of call for NATO's maritime research needs through our own expertise, particularly in the undersea domain, and that of our many partners in research and technology.

One of three research and technology organisations in NATO, NURC conducts maritime research in support of NATO's operational and transformation requirements. Reporting to the Supreme Allied Commander, Transformation and under the guidance of the NATO Conference of National Armaments Directors and the NATO Military Committee, our focus is on the undersea domain and on solutions to maritime security problems.

The Scientific Committee of National Representatives, membership of which is open to all NATO nations, provides scientific guidance to NURC and the Supreme Allied Commander Transformation.

NURC is funded through NATO common funds and respond explicitly to NATO's common requirements. Our plans and operations are extensively and regularly reviewed by outside bodies including peer review of the science and technology, independent national expert oversight, review of proposed deliverables by military user authorities, and independent business process certification.

NOTE: The NURC Reprint series reprints papers and articles published by NURC authors in the open literature as an effort to widely disseminate NURC products. Users should cite the original article where possible.

Tank measurements of scattering from a resin-filled fiberglass spherical shell with internal flaws

Alessandra Tesei,[a] Piero Guerrini, and Mario Zampolli
NURC, Viale San Bartolomeo 400, 19126 La Spezia, Italy

(Received 9 October 2007; revised 8 May 2008; accepted 23 May 2008)

This paper presents results of acoustic inversion and structural health monitoring achieved by means of low to midfrequency elastic scattering analysis of simple, curved objects, insonified in a water tank. Acoustic elastic scattering measurements were conducted between 15 and 100 kHz on a 60-mm-radius fiberglass spherical shell, filled with a low-shear-speed epoxy resin. Preliminary measurements were conducted also on the void shell before filling, and on a solid sphere of the same material as the filler. These data were used to estimate the constituent material parameters via acoustic inversion. The objects were measured in the backscatter direction, suspended at midwater, and insonified by a broadband directional transducer. From the inspection of the response of the solid-filled shell it was possible to detect and characterize significant inhomogeneities of the interior (air pockets), the presence of which were later confirmed by x-ray CT scan and ultrasound measurements. Elastic wave analysis and a model–data comparison study support the physical interpretation of the measurements. © *2008 Acoustical Society of America.*
[DOI: 10.1121/1.2945701]

PACS number(s): 43.30.Ky, 43.20.Fn, 43.20.Jr, 43.35.Zc [DF]

I. INTRODUCTION

Literature on nondestructive testing (NDT) for structural health monitoring (SHM) proposes several methods[1–5] based on the acoustic excitation and measurement of leaky surface-guided Lamb waves supported by thin plates made of metals and, more recently, with composite multilayered materials and bonded joints (see also a recent review article by Su *et al.*[6]). Acoustic inversion based on elastic scattering measurements either in air[7,8] or in water[9–11] is generally applied to thin plates of various materials, including composite laminates and plastics. Kinra *et al.*[12] presented a method for simultaneous health monitoring and inversion of the properties of the individual thin layers comprising a multilayered medium.

In this work, low- to midfrequency elastic scattering measurement and analysis are applied to water-loaded, finite objects with circular cross section (namely, solid spheres and spherical shells, either void or totally solid filled). Low- to midfrequency sound has been experimentally shown to penetrate into the metallic casing of an elastic object, and, hence, to provide information on its interior structure and content.[13,14] Here the purpose is to investigate whether elastic scattering can be significant (with respect to diffraction), and, consequently, exploitable for applications such as SHM and inversion, when the specimen to analyze is a finite object made with a dissipative, low-shear-speed material (i.e., a plasticlike material, possibly coated by a shell of composite, such as fiberglass). Unlike many recent works in NDT mentioned earlier, the goal here is the detection of internal flaws and the structural analysis of the material filling a composite shell, and not the SHM of the composite itself, which, in the selected bandwidth, is supposed to appear as a homogeneous medium.

As far as the inversion is concerned, the proposed technique takes advantage of the shape of the specimen. If compared to methodologies designed to invert the material properties of plates,[9–11,15] the insonification of an object with circular cross section allows the simultaneous excitation of all the elastic waves supported in a certain bandwidth through a single monostatic measurement, without the need for a bistatic measurement system and/or of the insonification at a fan of possible incident angles, as is generally done in the case of a flat interface. The resulting acoustic response is rich in information, but also more complicated to analyze, and, hence, requires model-based inversion.

Inversion is based on the analysis of the measured elastic echo structure, and on the application of an analytical model of scattering by layered elastic spheres. The approach can be easily extended to circular cylinders. The identification of each wave echo and the estimation of their times of arrival are exploited to feed the model with an initial guess of possible values for the bulk speeds of the material to invert. The estimate of the material bulk speeds derives from the minimization of the error between the measured and predicted scattering responses of the specimen. Similar acoustic inversion approaches, based on elastic scattering measurements of water-loaded shells with circular cross section, either void or liquid filled, can be found in the literature.[13,14] In these references, the material parameters were estimated by exploiting analytic relations with either the dispersion curves of the supported elastic waves or the periodicity of their time echoes. However, the identification of the elastic wave resonance modes in the spectral form function of the object can be nontrivial in the case of interference among closely spaced resonance modes, especially when the materials are

[a]Electronic mail: tesei@nurc.nato.int

dissipative, and, hence, many resonance modes are too weak to be detected. Moreover, the inversion methods based on the detection and identification in the time domain of a number of subsequent echoes for each wave are not applicable to dissipative media, for which only one echo per wave type is generally detectable. In these cases, a model-based approach exploiting the times of arrival of a few echoes is more widely applicable. However, being less accurate than resonance mode identification or estimation of echo periodicity, this wave analysis cannot be used to directly invert the parameters, but only to limit the search space.

Following a parametric study[16] conducted on thin-walled, totally filled spherical shells, with the purpose of investigating the effect of different fillers, acoustic measurements were performed on a fiberglass spherical shell filled with a low-shear-speed epoxy resin. Preliminary measurements were conducted also on the void shell before filling and on a solid sphere of the same material as the interior. The objects were selected to be simple enough to be treated by currently available modeling techniques, but realistic enough to give a first insight into the physics of the elastic waves present in such material combinations. The shell material is fiberglass consisting of layers of randomly distributed (hence approximately isotropic) "MAT" fiber. Acoustic data are in the range of 15–100 kHz, roughly corresponding to a *ka* range of 4–26 (with *k* being the water wave number and *a* the object radius), which is suitable for the excitation of a number of elastic waves. At these frequencies, a layer of randomly distributed fiber is assumed to be approximately isotropic and homogeneous, and sound is assumed to propagate in a multilayered composite shell as if it consisted of an homogeneous material. The same hypothesis can be made for the epoxy-resin filler, where air microbubbles can be trapped during manufacturing. Consequently, an analytical modeling tool is expected to be suitable to realistically predict the scattering response of a resin-filled fiberglass shell in a *ka* range of 4–26.[16] In this bandwidth, the elastic scattering component is expected to be significant despite the wave damping due to material dissipation.

The preliminary measurements of the solid resin sphere and of the void fiberglass shell were conducted to achieve, through acoustic inversion, an estimate of the constituent material parameters, namely of shear and compressional sound speeds and their attenuations.

Given the parameter estimates of the constituent materials, the measurement of the resin-filled fiberglass shell aimed to verify whether the elastic waves predicted by analytical models were detectable and to check its general structural health. It was also addressed to investigate whether perfect contact at the filler–shell interface (as assumed in past simulation studies[16]) was achieved during manufacturing. This analysis revealed inhomogeneities of the interior (in particular an extended air pocket having a quasisymmetric annular shape), which were later confirmed by x-ray CT scan and high-frequency ultrasound spot measurements. The air pocket was presumably caused by a local detachment of the resin filler from the shell during the solidification process. Estimation of the geometry of the main air pocket was useful for obtaining a more accurate model of the object. The AXISCAT modeling tool recently developed at NURC[17] was used to generate the backscattering response of the filled spherical shell, including the air pocket.

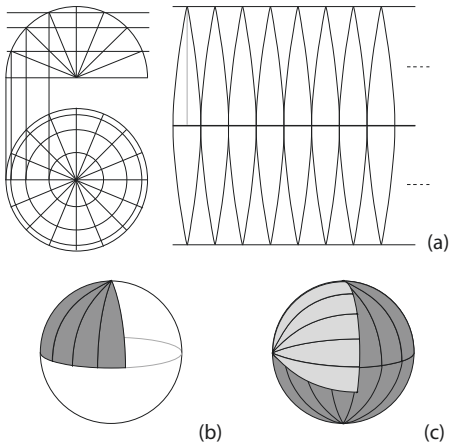

FIG. 1. Schematics of the main steps of the manufacturing process of the fiberglass shell. (a) Two-dimensional projection of a spherical surface according to the Monge method; (b) building of the first layer of the shell by positioning the spindle-shaped fiber patches (dark gray) over a glass mother shell (white); and (c) positioning of the next layer of patches (light gray) according to an orthogonal orientation with respect to the previous one.

The paper is organized as follows. Section II provides details on the manufacturing of the spherical objects, on the tank facility, and on the experiments conducted. The theoretical background for elastic wave analysis is briefly described in Sec. III, and the acoustic data are discussed in Sec. IV, along with the inversion results. A detailed analysis of the resin-filled fiberglass shell is reported in Sec. V, including additional NDT measurements and results of the model–data comparison. Conclusions are presented in Sec. VI.

II. DESCRIPTION OF THE SPHERICAL OBJECTS AND OF THE MEASUREMENT SETUP

The manufacturing constraints on the shell were: (i) to have approximately uniform thickness (within 0.5 mm over a wall thickness of 2.5 mm) and uniform radius curvature (within 1.5 mm over a nominal outer radius of 62.5 mm), and (ii) to have a material as homogeneous and isotropic as possible along the surface and through the wall thickness. To achieve this, a MAT random fiber (namely, MAT 300) was used, cut in a set of spindle-shaped patches according to the planar representation of a hemispherical surface obtained through the Monge method (or method of double orthogonal projections), as shown in Fig. 1(a). Figures 1(b) and 1(c) describe how each spherical layer of fiber was built by mosaicking the set of spindles over a thin glass shell in order to reconstruct a spherical surface by totally covering it without overlapping. At each layer, the orientation of the patches was changed [see Fig. 1(c)], in order to minimize the effect of joints at the sides of the patches themselves. After the solidification of the first layer, the mother glass shell was broken and extracted from the interior through a small hole. The sphericity was checked for layer after layer while the matrix was still liquid; at the end of the process, the sphericity was ensured by polishing. The percentage of glass with respect to resin was kept around 50%.

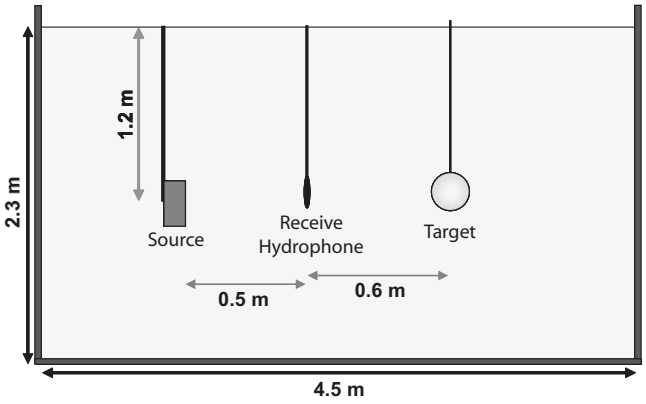

FIG. 2. Geometry of the tank measurement setup (not to scale).

The epoxy resin used as a solid filler was originally liquid; in order to maintain an isothermal chemical reaction during the curing process, it was cast layer by layer in about five steps, given the sphere size, each layer needing a predefined time to solidify. In order to build an uncoated solid sphere the resin was cast into a thin-walled glass spherical shell, which was broken and removed at the end of the process. A final smoothing ensured the sphericity also around the shell filling hole. The same step-by-step casting procedure was adopted to fill the fiberglass shell through a small hole (about 5 mm diameter) in the shell itself, which was closed at the end with some resin.

The measurements were conducted in the NURC tank, which is 4.5 m × 3 m × 2.3 m, has steel walls and bottom, and is filled with fresh water. For suspension, the objects were placed in a thin nylon wire net, fixed to the object by several resin drops (having a maximum diameter of about 10 mm and an average maximum thickness of about 0.5 mm). Whereas the filled objects were suspended through a thin nylon wire, as shown in Fig. 2, the hollow, buoyant shell was connected through a nylon wire to a lead weight placed on the floor of the tank. The source (Reson TC2138) was located at midwater at one end of the tank. Although its sensitivity is roughly flat between 40 and 100 kHz, the high signal-to-noise ratio made it possible to obtain useful data from about 15 to 100 kHz. The receiver was an omnidirectional hydrophone with a roughly flat response between 1 and 300 kHz. As shown in Fig. 2, it was located on the transmission axis between transmitter and target in such a way as to minimize the surface and bottom interference. This constraint made it necessary to locate the object at about 1.1 m from the transducer and at about 0.6 m from the hydrophone, which are distances theoretically insufficient to guarantee a plane wave insonification at frequencies lower than 50 kHz (roughly corresponding to $ka=13$), and a far field measurement of the object scattering at frequencies lower than 57 kHz ($ka\approx 15$). In the modeling phase of this study, the incident field is approximated by a plane wave for simplicity, while the actual distance between object and receiver is taken into account. Model–data comparison results follow, which show that the plane wave approximation is applicable. The directionality of the source (having 30° of beamwidth null to null at 50 kHz and sidelobes −20 dB down) allowed the complete illumination of a target without strong interferences with the tank boundaries and the water surface. The residual reverberation was mitigated by subtracting a coherent average of 20 pings of scattering from the tank boundaries. Data were coherently averaged over 20 pings and equalized in the spectral domain by using the direct measurement of the transmitted pulse on the same hydrophone. The target strength data were Hamming windowed before applying an inverse Fourier transform in order to get a smooth time response.

III. ELASTIC SCATTERING THEORY FOR LOW-SHEAR-SPEED MATERIAL SPHERICAL SHELLS

The theoretical basis for the interpretation of the scattering measurements derives from wave analysis applied to simulated far-field backscattering by fluid-loaded spheres insonified by a plane wave in the free field. The most general case considered is scattering by a solid-filled spherical shell made of possibly lossy materials. The analytical scattering model uses a standard expansion[18] for the scattered field P_{sc} into a partial wave series at range r and angle θ,

$$P_{sc}(r,\theta)=\sum_{n=0}^{\infty} i^n(2n+1)a_n h_n^{(1)}(kr)P_n(\cos(\theta-\theta_{inc})), \quad (1)$$

where h_n are the outgoing spherical Hankel functions, P_n are the Legendre polynomials, θ_{inc} is the angle of the incident plane wave, and a_n are the coefficients to be determined. These coefficients, and the coefficients of the field expansion in the solid layers of the sphere, are determined by applying the appropriate continuity conditions at the interfaces. In particular, the model assumes perfect contact at the filler–shell interface. It is convenient to determine the coefficients a_n by Cramer's rule, from which

$$a_n = B_n/D_n, \quad (2)$$

where B_n and D_n are two determinants, the elements of which are reported for example by Veksler[18] for a solid sphere, by Kargl *et al.*[19] for a void spherical shell, and can be computed for a solid-filled shell in a way similar to what is reported in these references. The backscattered field is obtained by imposing $(\theta-\theta_{inc})=\pi$ in Eq. (1).

Wave analysis consists in the identification of the elastic waves supported by the scatterer, and in the study of their properties in terms of phase (and group) speed dispersion curves, and attenuation. This is achieved by studying the modal coefficients a_n as the wave number k, and, hence, the frequency f, varies. For a given n, the lth maximum of a_n locates the nth-order resonance frequency of the lth elastic wave, f_n^l. The corresponding wave phase speed is computed by

$$c_{ph}^l = 2\pi f_n^l a/(n+1/2), \quad (3)$$

and its group speed can be approximated by[7]

$$c_g^l \approx 2\pi(f_n^l - f_{n-1}^l)a. \quad (4)$$

The attenuation of the wave modes as frequency varies is studied through the Sommerfeld–Watson transformation.[20] A numerical method, developed for solid spheres by Williams *et al.*[21] and for void spherical shells by Kargl *et al.*[19] and

TABLE I. Material parameters.

	c_p (m/s)	c_s (m/s)	α_p (dB/λ)	α_s (dB/λ)	ρ (kg/m^3)
Water	1490		0		1000
Fiberglass	3500	1560	0.3	0.7	1530
Epoxy resin	3000	1550	0.8	1.8	1845
Steel	5950	3240	0	0	7700

working under free field conditions, has been extended here to lossy materials and applied to give an indication of the damping of the supported elastic waves due to both radiation and material absorption. The method, for a fixed ka value, solves

$$D_{\nu^l}(ka) = 0, \tag{5}$$

where D_{ν^l} is the denominator of Eq. (2), after replacing the real modal order n^l with its complex version

$$\nu^l = n^l + i\beta^l, \tag{6}$$

according to the Sommerfeld–Watson method. The complex modal order ν is the unknown of the equation. Its imaginary part β^l represents the damping of the elastic wave when it propagates along a circular arcpath corresponding to a unit central angle. It includes radiation damping and material absorption. Because it is based on an extension of the geometric diffraction theory to elastic phenomena,[20] this approach is valid for mid to high-ka values; in this study it is applied for a minimum ka of 5.

Hefner and Marston[22] proposed an alternative approximated formula for the damping factor of the elastic waves supported by solid spheres made of lossy materials:

$$\beta^l \approx \beta^l_{\text{lossless}} + \gamma^l\left(\frac{ka}{c^l_{\text{ph}}/c^{\text{ext}}} - 1/2\right), \tag{7}$$

where $\beta^l_{\text{lossless}}$ is the radiation damping factor that derives from the solution of Eq. (5) with real wave numbers. The symbol γ^l represents the imaginary part of the complex wave number of the lth wave supported by a water-loaded elastic half-space having the same properties as the dissipative material of the sphere. This is an alternative to solving Eq. (5) with complex bulk speeds, and is particularly interesting when the quality factor of a wave becomes too low due to material dissipation to allow the exact method to converge. Here the exact method is applied, except where otherwise indicated.

The analysis is performed over a ka range ($ka \leqslant 150$) much broader than what could be measured in the tank, with the purpose of making the theoretical study more complete, by including a large set of elastic waves and giving an idea of their asymptotic behavior, and, hence, of their general nature. The wave analysis is first applied to the components of the solid-filled shell of interest, namely (i) a void spherical shell made of fiberglass and (ii) a solid sphere made of the same epoxy resin as the filler. This helps in understanding the basic physical phenomena involved. The values of the material parameters used for the simulations are listed in Table I. The sound speed c^{ext} of the loading water was measured in the tank during the experiments. The values chosen for the material parameters are those estimated from the acoustic inversion of the fiberglass (for the external casing) and of the epoxy resin (for the solid filler), as presented in Sec. IV. The speed values are similar, but the attenuations are much bigger in the resin than in the fiberglass. One can notice that the values of the shear speed are supersonic, but very close to the sound speed in water. In a previous parametric study,[16] the shear speed turned out to be the parameter that mostly influences the classification of a material in terms of its elastic behavior. In particular, it is customary[23] to classify a material as plasticlike if its shear speed is subsonic with respect to loading water and its density is close to the water density and as metal-like if its shear speed is supersonic and its density much higher than the water density. In fact, it would be preferable to classify as plasticlike a material having the Rayleigh speed subsonic (even if its shear speed is supersonic), since it has been shown[16] to support the Scholte–Stoneley wave as a plastic material does.[24] For material classification purposes the Rayleigh speed considered is the speed of the Rayleigh wave supported by a free half-space. For plastic materials, both compressional and shear waves are generally highly damped.

The materials used in this experimental work fall within the category of plasticlike materials, since their shear speed is slightly supersonic, but their Rayleigh speed is subsonic. Furthermore, both the compressional and shear waves are significantly damped, and the density is close to water density, compared to the density of metal-like materials.

Figure 3(a) shows the wave analysis of the void shell with thickness $d=0.04a$ in terms of phase speed dispersion curves (upper plot) and damping factor β (lower plot) of the waves supported by the structure. The sphere geometry is the nominal geometry of the fiberglass shell measured in the tank, i.e., outer radius equal to 62.5 mm, and wall thickness 2.5 mm. For comparison, Fig. 3(b) shows similar results for a void steel shell of the same size and thickness (see Table I for the steel properties). The differences between the dispersion curves for the two materials are evident. In plastic shells, the A_{0-} Lamb-type wave is not supported, and the so-called coincidence frequency[25,26] does not exist. The other Lamb-type waves exist in both cases, but with very different asymptotic behaviors. As they are shear in nature, in plastic the S_0 and all the A Lamb-type waves tend relatively rapidly to the shear speed, which is generally slightly supersonic or subsonic. In metal, they are known to tend to the Rayleigh speed value in the mid to high-ka range and, at very high ka, to tend asymptotically to the bulk shear speed. For this reason, for example, in plastic the speed of the A_{0+} wave varies rapidly at low ka, then exponentially decays toward the material's low shear speed and becomes almost nondispersive; in metal, beyond the coincidence frequency, it increases with frequency and is highly dispersive. In the fiberglass shell, the only wave that significantly contributes to scattering, and for which the damping factor can be computed, is the S_0 wave. The other waves predicted are so highly attenuated that they cannot be detected at all over the bandwidth. The damping curves are shown for $\beta < 3.5$, since for β values even just slightly larger than 1, the resonance modes cannot be detected in the target response. In steel, the S_0 wave, being

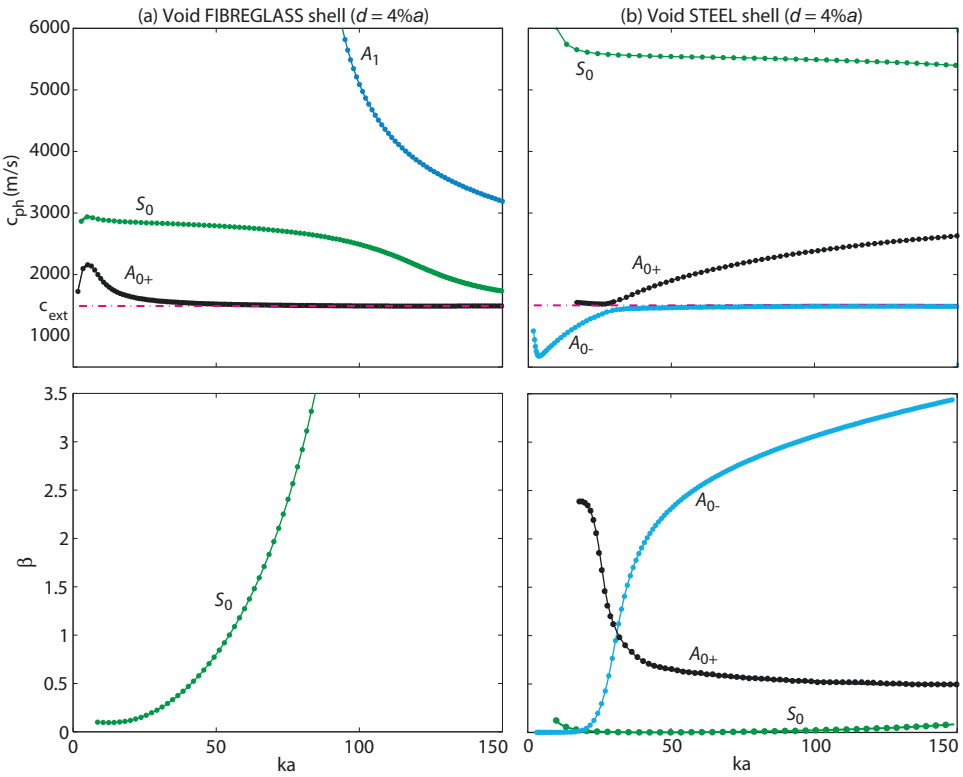

FIG. 3. (Color online) Wave analysis applied to a void, thin-walled shell made of fiberglass (a) and of steel (b). The upper plots show the phase speeds of the supported waves, as predicted by analytical modal analysis; the dash-dotted line indicates the sound speed in the external fluid. The lower plots show the damping factor β, as estimated by the numerical method originally introduced by Kargl *et al.* (Ref. 19). The numerical method is not able to estimate the damping factor of some of the waves due to their high attenuation. Their excitation is predicted by the theoretical scattering model, but they cannot be observed. The dot markers localize the resonance modes of each wave.

almost nondissipative in nature, has a very low damping factor, which remains almost flat over the whole bandwidth; in fiberglass, its damping rapidly increases due to intrinsic material dissipation. As is well known,[25] the A_{0+} and A_{0-} waves in steel exchange their nature around the coincidence frequency, which is located here around $ka=30$, depending on the shell-wall thickness and the material parameters.[27]

The second basic case is a water-loaded solid sphere, either made of epoxy resin as measured in the tank [Fig. 4(a)] or, for reference, made of steel [Fig. 4(b)]. The phase speed dispersion curves and the attenuation factor are predicted for the waves supported by solid spheres of outer radius 60 mm, which is the nominal outer radius of the measured solid sphere. The dashed lines connecting modes of the dispersion curves of some Whispering–Gallery waves indicate that the modes in between are missing due to their extremely high attenuation. The subsonic Scholte–Stoneley wave is excited only in the plasticlike sphere, and is expected to dominate the response at $ka<30$, beyond which its damping starts to increase. Its dispersion curve asymptotically tends to the Scholte–Stoneley speed computed for a water-loaded half-space and shows that the wave is nondispersive for $ka>10$. The Whispering–Gallery waves of longitudinal type asymptotically tend to the material compressional speed; the Whispering–Gallery waves of transverse type and the Rayleigh wave tend to the shear speed. Although the Rayleigh speed in a free half-space made with the same resin is predicted to be subsonic ($c_R \approx 1400$ m/s), the Rayleigh wave in the water-loaded resin sphere is slightly supersonic. In the steel sphere, the compressional speed is so high that the longitudinal waves are not included in the dispersion plot of Fig. 4(b). Their modes interfere so strongly with the transversal Whispering–Gallery wave modes that they are very difficult to identify and analyze. For this reason, the damping factor of the first-order longitudinal Whispering–Gallery wave is predicted by the approximated method proposed by Hefner and Marston.[22] The Whispering–Gallery waves and the Scholte–Stoneley wave are almost nondissipative in nature. Their strong damping in the resin sphere is mostly caused by material attenuation: At mid to high-ka values, the slope of the damping curves changes and tends to the damping they would respectively have if they traveled in a water-loaded half-space of the same resin as the sphere.[22] Studies on the Rayleigh wave at solid–fluid interfaces[23] showed that it is leaky in metals, as confirmed by the trend of its damping factor for steel, but it is unleaky in plastics. This cannot be confirmed by the analysis in this paper, since, for the epoxy-resin sphere, its damping factor cannot be evaluated.

The effect of a fiberglass, thin-walled shell coating a resin solid sphere is weak,[16] if the contact at the interface is perfect (i.e., continuity is satisfied for all the components of stress and displacement). This is due to the thin walls and the very similar properties of the two materials. In this case the shell is practically transparent, especially at low to mid-ka. For this reason a complete wave analysis is not reported for the resin-filled fiberglass shell. The dominating waves scattered by the solid-filled shell are the same as predicted by a solid sphere of the same size made of the filler material.[16] The filler-borne Whispering–Gallery waves of longitudinal and transverse types are unaffected by the shell over the entire bandwidth.

In a coated sphere, the Scholte–Stoneley and the Rayleigh surface waves travel at the interface between two solids, and not, as for the solid sphere, at the interface between the solid and water. However, with the combination of the two materials investigated and a shell sufficiently thin, this

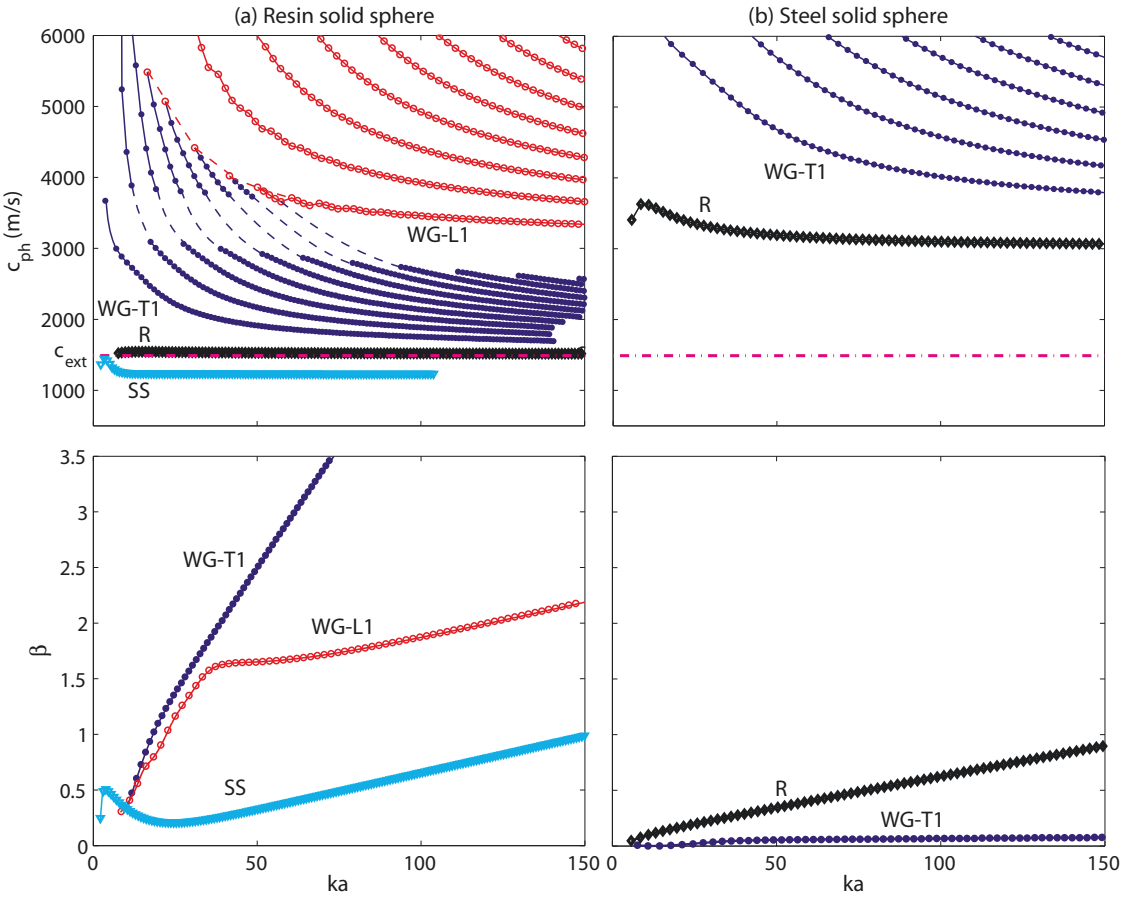

FIG. 4. (Color online) Wave analysis applied to a solid sphere made of an epoxy resin (a) and with steel (b). The upper plots show the phase speed dispersion curves of the supported waves, as predicted by analytical modal analysis. The dash-dotted line indicates the sound speed in the loading fluid. The lower plot shows the waves' damping factor. All the curves with closed circles in the upper plots refer to Whispering–Gallery waves of transverse type (labeled as WG-T), all the curves with open circles refer to the Whispering–Gallery waves of longitudinal type (WG-L). Only the first-order waves of the two types are labeled as they are the only ones contributing to backscattering. For the same reason, the damping factor is computed only for these two waves. The label R stands for Rayleigh wave and the label SS for Scholte–Stoneley.

has shown not to affect their properties. In particular, Fig. 5 shows the phase and group speed dispersion curves predicted for the Scholte–Stoneley and Rayleigh waves in the case of the fiberglass-coated and uncoated solid resin sphere studied in Fig. 4. It should be noticed that in this case the Scholte–Stoneley wave is expected to provide a strong contribution to the object response, while the Rayleigh wave is expected not to be seen. For other material combinations, theoretical and experimental studies[28] demonstrated that both waves can simultaneously propagate, and that they can simultaneously be observed. Under conditions of perfect bonding, the damping factor of the Scholte–Stoneley wave is negligibly affected by coating, and, hence, it is not reported here. If the contact is not perfect, the Scholte–Stoneley wave was found to undergo strong attenuation and dispersion, depending on the type of contact. The bonding types most commonly studied in the literature are the pure transverse slip,[29] and those boundary conditions characterized by discontinuity of either tangential[30] or radial, or both displacements.[31]

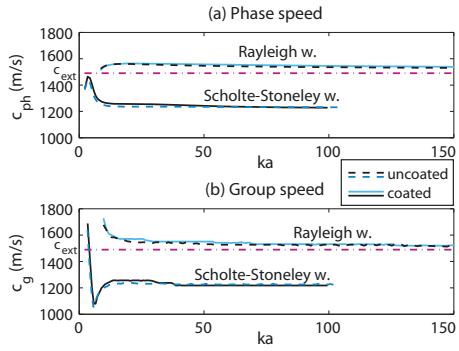

FIG. 5. (Color online) Phase (a) and group (b) speed dispersion curves of the Scholte–Stoneley and Rayleigh waves predicted for a solid resin sphere either uncoated or coated by a thin fiberglass shell (d=4%a). The dash-dotted line indicates the sound speed in the loading fluid. Perfect contact is assumed between the shell and the filler in the coated sphere. Due to the similar properties between the two materials and the thin walls of the casing the two waves are predicted to be negligibly affected by the presence of the shell.

Acoustic inversion procedure. The block diagram in Fig. 6 describes the inversion procedure applied to estimate the target material parameters either for a void shell or for a solid sphere. As suggested by previous investigations[16] and by the theoretical considerations presented earlier, this approach could be applied also to a completely filled, thin-walled shell in order to estimate the properties of the filler material. The approach can be easily extended to specimen of cylindrical shape having length significantly bigger than the radius.

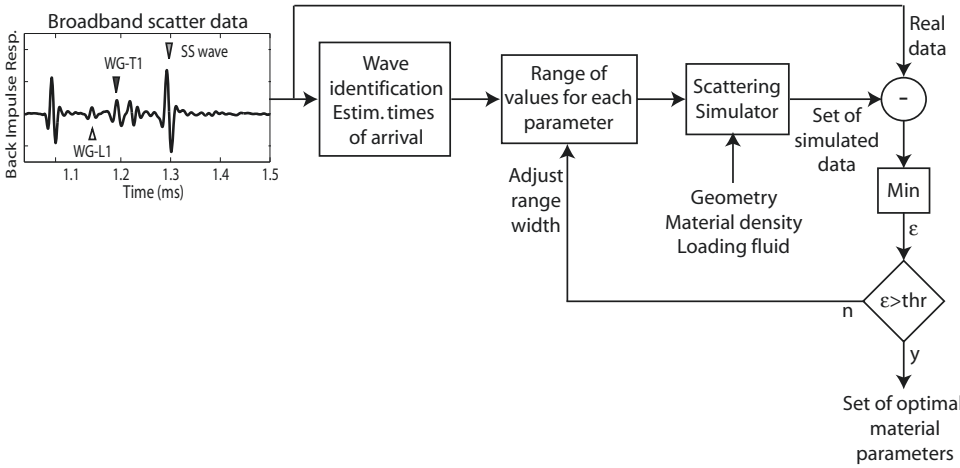

FIG. 6. Block diagram of the procedure applied to backscatter target response to invert a set of unknown material parameters.

The core of the approach is an analytical modeling tool for scattering by a free-field, fluid-loaded sphere based on Eq. (1). Hence, the materials are assumed to be homogeneous and isotropic, and the hypothesis of plane wave insonification is applied. Measurement geometry (i.e., sphere radius and thickness, and receiver position), loading fluid, and material density should be *a priori* known. Precision in the knowledge of the sphere's thickness and radius curvature should be on the order of about five-hundredths of a wavelength. This tolerance is generally achieved in standard manufacturing processes which are based upon the addition of successive layers of fiber, starting from a mother shape. Such processes are customarily implemented by specialized companies, such as those operating in the construction of high-end sail and motor yachts. The simulator must also be fed with a value for each of the unknown parameters. A range of possible values for each parameter is forecast based on the analysis of the measured scattered data, from which the time of arrival of each wave echo can be estimated. The delay Δt_m^l of the mth echo of the wave l with respect to the time of arrival of the front echo is related to the group and phase speed of the wave (c_{g}^l and c_{ph}^l respectively) as follows:[19]

$$\Delta t_m^l = 2a\left[\frac{1-\cos(\theta_{\mathrm{c}}^l)}{c^{\mathrm{ext}}} + \frac{\pi-\theta_{\mathrm{c}}^l+m\pi}{c_{\mathrm{g}}^l}\right], \tag{8}$$

where $m=0,1,2,\ldots$ is the number of complete circumnavigations, and $\theta_{\mathrm{c}}^l=\arcsin(c^{\mathrm{ext}}/c_{\mathrm{ph}}^l)$ is the wave coupling angle. The values of c_{g}^l and c_{ph}^l (hence of θ_{c}^l) generally vary with respect to frequency; the frequency value used in Eq. (8) is the middle frequency of the band. In turn, the phase and the group speed of a wave varies with the material compressional and/or shear speeds, depending on the nature of the wave analyzed (as discussed for example by Viktorov[32]). The forecast is more precise, and, hence, the range of possible values more limited, when nondispersive waves are supported, as their phase and group speeds do not depend on frequency. Knowing the kind of material (namely either metal/stone or plasticlike) helps to predict what kinds of waves will be excited, and hence helps in the wave identification process, which is an essential preliminary phase of the inversion method. When several elastic waves are excited (such as in a solid sphere or in a very broadband measurement), the parameter estimation becomes more precise, due to redundancy of information. The wave attenuations are very difficult to predict from data analysis, and, hence, their possible ranges of values are kept wide.

Given the range of the search domain for each unknown, a simulated response for each combination of parameters is computed. The functional given by the difference between measured and simulated impulse responses in a certain bandwidth is minimized to obtain a set of optimal parameters. Until the minimum achieved exceeds a fixed threshold, the simulation/minimization process is iterated by feeding the simulator with a wider range of values for each unknown parameter. In order to keep the problem size relatively small, the customary procedure is to invert the compressional and shear speeds of the material, keeping their respective attenuations fixed to reasonable numbers. Once the two speeds are estimated, a new inversion procedure is applied to estimate their attenuations. The two problems can be separated because the attenuation values affect the amplitudes of the elastic wave echoes, but only negligibly their times of arrival, which, instead, are directly related to the compressional and shear speeds of the material.

IV. ACOUSTIC TANK MEASUREMENTS

Preliminary tests of homogeneity of the materials at the frequencies of interest were conducted by measuring the backscattering at different aspects of insonification, evaluated with respect to arbitrary zero references, as sketched in Fig. 7. First, backscattered responses by a void fiberglass spherical shell (outer radius $a=62.5$ mm, thickness $d=2.5$ mm) and by a solid sphere of epoxy resin (radius $a=60$ mm) were measured with the target suspended in midwater. In the investigated bandwidth, the shell appeared homogeneous (Fig. 8 compares measurements at aspects 45° and 180°). At the two ends of the investigated bandwidth (i.e., for $ka<7$ and $ka>20$), discrepancies are possibly due to the lower SNR level at the extremes of the source bandwidth. In the considered bandwidth, only the S_0 Lamb-type wave can be detected, as anticipated in Sec. III. The exponential decay of the amplitudes of its echoes is evident in the time responses.

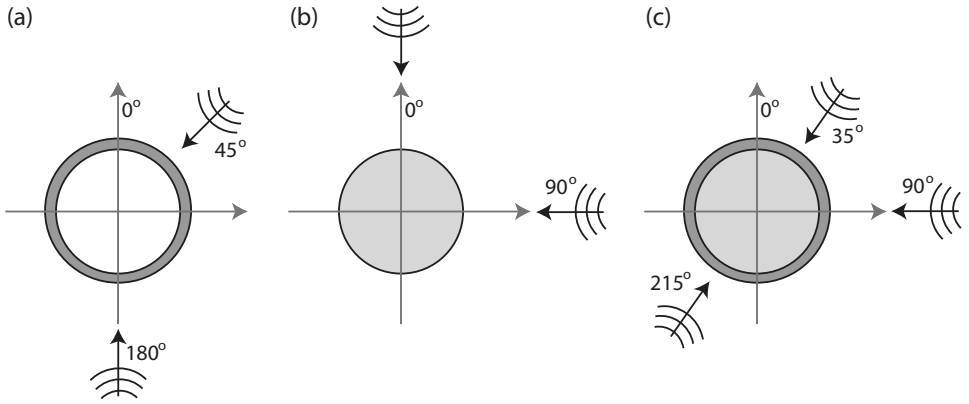

FIG. 7. Geometry of the measured spheres and respective insonification angles: (a) Void fiberglass shell; (b) solid epoxy-resin sphere; and (c) resin-filled fiberglass shell. Geometry is not to scale.

Figure 9 shows the data comparison of the solid resin sphere insonified at two different aspects. Although the resin was cast in a set of steps during the sphere manufacturing, as described in Sec. II, from the data agreement between different aspects of insonification one can deduce that the sphere is homogeneous in the bandwidth. The orientation of the interfaces between adjacent layers of the filling resin with respect to the direction of insonification is unknown. Wave identification can be applied only in the time domain, since the target strength is dominated by the strong interference between the specular and the Scholte–Stoneley echoes, which hides all the resonance modes. The impulse response is dominated by the first echo of the Scholte–Stoneley wave, which is expected to be the strongest elastic wave supported at low- to mid-*ka*. The first echoes of the first-order Whispering–Gallery waves of longitudinal and transverse types, respectively, can be identified. The latter one is very dispersive in this bandwidth, as predicted by its dispersion curve in Fig. 4.

The resin-filled shell was measured under the same geometry at different aspects of insonification. The comparison of time responses between aspect 35° and 90° is shown in Fig. 10(a), and between aspects 90° and 215° in Fig. 10(b). The main elastic wave echoes are identified. The response at 35° shows phase reversal of the front echo. Small differences in amplitude and phase are related to the various Whispering–Gallery wave echoes. As in the solid sphere data, the transversal Whispering–Gallery echo is very dispersive. The most significant changes among the different measurements appear in the amplitude, phase, and dispersion of the first Scholte–Stoneley wave echo. In particular, the Scholte–Stoneley wave echo is bigger and less dispersed at 35° of insonification, i.e., when the front echo is reversed. Data at aspect 215° is perfectly in phase with the ones at aspect 90°, but the Scholte–Stoneley echo has almost disappeared and new significant echoes can be seen around 1.35 ms, possibly reflected/diffracted by local, sparse inhomogeneities. The phase reversal of the front echo in the data at aspect 35° suggests the presence of a considerably extended air bubble or air layer immediately behind the part of the shell hit by the incident pulse. In the data at aspect 90° and 215°, the filler appears in contact with the shell in the illuminated part of the sphere (front), whereas the lower level of the Scholte–Stoneley wave echo may indicate, as expected by theory,[29–31] that under these geometries the air pocket is in the rear part, where this wave travels before its first back reradiation. Hence, the sphere is evidently neither three-dimensional (3D) symmetric nor homogeneous, due to the presence of one or more extended air pockets, which are

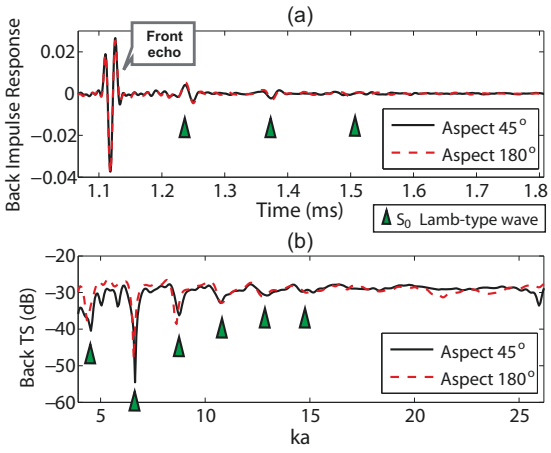

FIG. 8. (Color online) Comparison of backscattered response by the void fiberglass shell at two different aspects: (a) Time impulse response and (b) target strength. Elastic wave identification is superimposed.

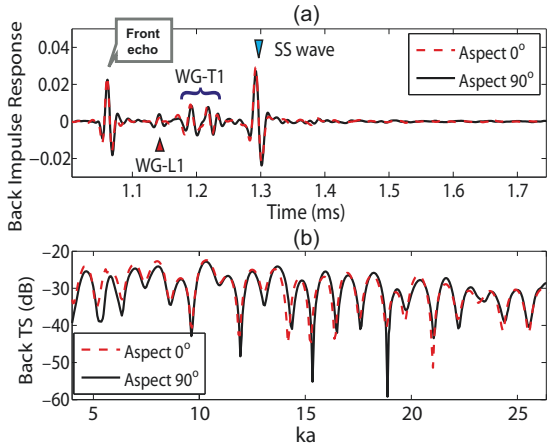

FIG. 9. (Color online) Comparison of backscattered response by the solid resin sphere at two different aspects: (a) Impulse response and (b) target strength. Elastic wave analysis is applied to the impulse response: WG-L/T1 represent longitudinal/transverse Whispering–Gallery waves of the first order; SS represents Scholte–Stoneley wave. The strong interference between the specular echo and the first Scholte–Stoneley wave echo does not allow the identification of wave resonance modes in the frequency domain.

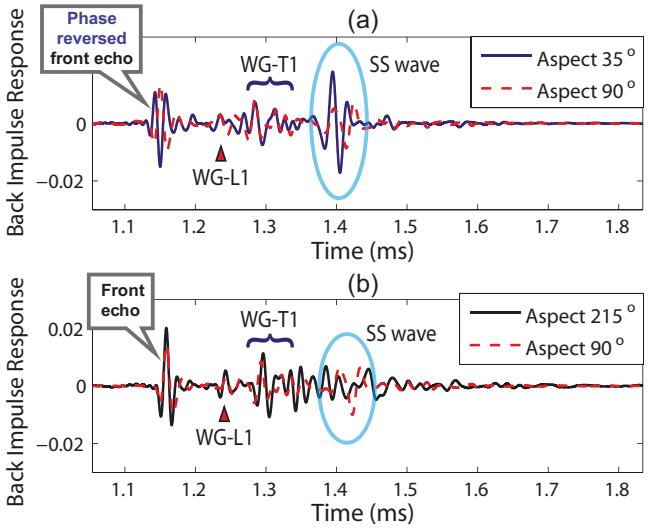

FIG. 10. (Color online) Backscattered impulse response by the resin-filled fiberglass spherical shell at different insonification aspects: Comparison between angles 35° and 90° (a), and between angles 90° and 215° (b). Wave analysis is superimposed.

expected to be located at the interface between solid and shell, as they strongly affect only the Scholte–Stoneley surface wave.

Acoustic inversion of material properties based on elastic scattering features. Acoustic inversion is applied to the void shell and the solid sphere in order to estimate the elastoacoustic parameters of their materials in the studied frequencies. The inversion methodology used is described in Sec. III. The material densities are estimated by measuring the weight and by estimating the volume of the objects. Figure 11 shows the result of model–data comparison for the void shell in the time and frequency domains after acoustic inversion of the material parameters. The inversion results are indicated in Table I. The estimation error on the speeds is

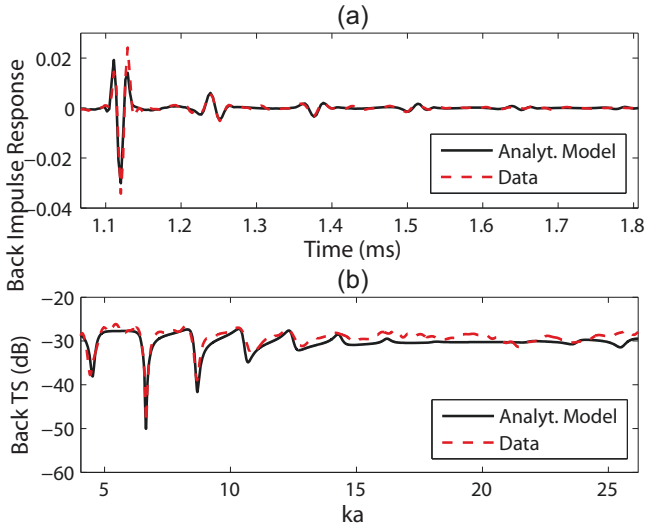

FIG. 11. (Color online) Model–data comparison of backscattering by the void shell. The analytical model is applied. Data were measured at aspect 180° (see Fig. 8). The plots show the model–data comparison of (a) the impulse response and (b) the target strength. The model is fed with the material parameters obtained from the inversion process and listed in Table I.

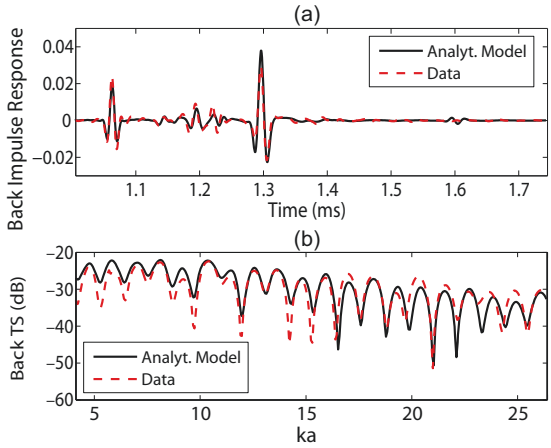

FIG. 12. (Color online) Model–data comparison of backscattering by the resin solid sphere (analytical model is applied): (a) Impulse response and (b) target strength. The model is fed with the material parameters obtained from inversion and reported in Table I.

of the order of ± 30 m/s, on the attenuations around ± 0.2 dB/λ. The disagreement beyond $ka=15$ is possibly due to increasing relevance of the fiber structure details as the frequency increases, which may perturb the propagation of the S_0 wave, being shell-borne and surface guided in nature. The relatively high uncertainty of the estimate derives from the excitation of only one elastic wave in the measured bandwidth and from the fact that, in this band, its phase speed derives from a combination of the bulk compressional and shear speeds of the material.[26]

The model–data comparison achieved after acoustic inversion of the solid sphere data (Fig. 12) shows a generally good agreement. The inversion results are indicated in Table I. The estimation error of the two speeds is of the order of ± 20 m/s, lower than in the shell case since here more elastic waves are excited, providing redundant information, hence more robust estimation. The very good agreement achieved between model and data suggests that the model approximation of assuming plane wave insonification is acceptable also for $ka<13$. It also seems to suggest that the material is nondispersive in the whole bandwidth of interest. The main discrepancy in the time-domain model–data comparison is in the level of the Scholte–Stoneley surface wave echo arriving at $t=1.3$ ms, and corresponding to a mismatch in the target strength level, mainly at low ka. This is probably due to partial diffraction (and, hence, leakage) of the wave at the small protrusions of the suspension system.

The estimated values of the two bulk speeds are in very close agreement (within a few tens of m/s) with the results obtained from ultrasonic spot measurements. These measurements were conducted at 2 MHz (for compressional speed measurement) and at 5 MHz (for shear speed measurement) on a 10-mm-thick, flat disc specimen made of the same material. Nevertheless, this is not sufficient to conclude that the material is nondispersive over a bandwidth ranging from 100 kHz up to frequencies of the order of 1 MHz, since the frequency dependence of the phase velocity (and attenuation) of ultrasonic waves in an epoxy resin was experimentally shown to depend on the curing process.[33]

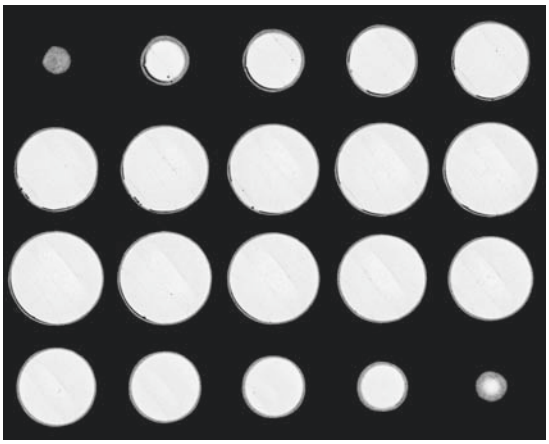

FIG. 13. Sequence of a subset of CT-scan vertical slices of the resin-filled fiberglass shell (horizontal resolution subsampled to 6.25 mm).

V. DETAILED CHARACTERIZATION OF THE SOLID-FILLED FIBERGLASS SPHERICAL SHELL

The detection of a considerably sized air layer at the solid–shell interface of the totally filled sphere induced the authors to conduct independent measurements aimed to localize and characterize it.

A. Additional NDT measurements and estimation of the air-pocket geometry

Confirmation of the presence of an extended thin air pocket between shell and filler comes from additional independent measurements. The x-ray CT scan of the sphere, performed with a GE Medical Systems multislice scanner at the Radiology Branch of the Carrara Hospital, has a horizontal resolution of 0.625 mm and reveals the presence of an extended interlayer of air below the shell, along with sparse air bubbles of different size, and various small patches of heterogeneous material (possibly corresponding to small bubble clouds or blobs of different density) within the filler. An example of data acquired is given by the sequence of a subset of CT scan images in Fig. 13. From the analysis of the slices, it is also possible to check the sphericity of the object and the uniformity of the shell wall thickness. In the first and last slices of the sequence, the small gray-scale texture of the images reveals the composite nature of the shell material; however, it also appears relatively homogeneous, since no joint between adjacent fiber patches can be distinguished. A detailed analysis of one of the most significant slices is provided in Fig. 14. The image clearly shows the section of two air pockets which are almost symmetric with respect to an ideal symmetry axis superimposed on the image. Their thickness is maximum (about 1.5 mm) close to pole P and then gradually decreases to zero closer to the equator. Visual inspection allows also the detection of the interfaces between the different layers of the casting process, all approximately perpendicular to the symmetry axis. The application of some basic image processing procedures allows the 3D reconstruction of the air pocket, as shown in Fig. 15, where the shell is rendered as semitransparent and the air bubbles and the air pocket are opaque. The roughly symmetric annular shape of the air interlayer is evident. From a slice-by-slice analysis

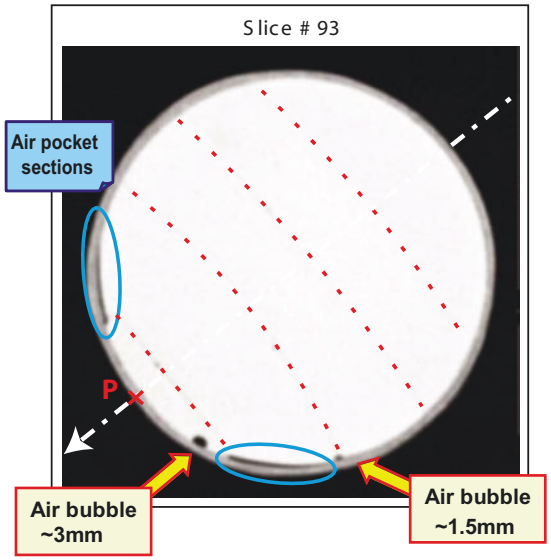

FIG. 14. (Color online) Analysis of one significant CT-scan vertical slice. The image background is black, the shell midgray, the filler light gray. The air bubbles/pockets appear black or dark gray in the x-ray image. The superimposed dotted lines localize the interfaces between adjacent cast layers of the filling resin. The dashed-dotted arrow shows a virtual axis of symmetry. The pole P, marked by a cross on the axis of symmetry, roughly corresponds to the filling hole. The main air-pocket cross sections, roughly symmetric with respect to the drawn axis, are surrounded by ellipses.

and from the 3D reconstruction it is possible to deduce that the air pocket was caused by the shrinkage of the inner material during the solidification of the fourth casting step. During the following, and last, casting step the resin could not fill the thin gap as some air remained trapped. The 3D reconstruction also shows that several big air bubbles remained trapped during the last casting step very close to the small hole through which the shell was filled.

In order to better measure the extent of the ring along the sphere surface, ultrasound scanning was conducted at 5 MHz with a Krautkramer transducer on the surface of the

FIG. 15. (Color online) Three-dimensional reconstruction of the resin-filled shell from x-ray CT scanning. The sphere shell is confined between two semitransparent surfaces, while the trapped air is enclosed within opaque surfaces.

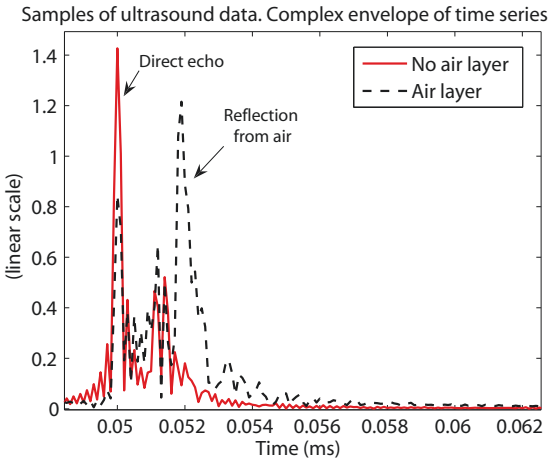

FIG. 16. (Color online) Ultrasound measurement of the resin-filled shell. Example of signals in presence and absence of an internal air bubble.

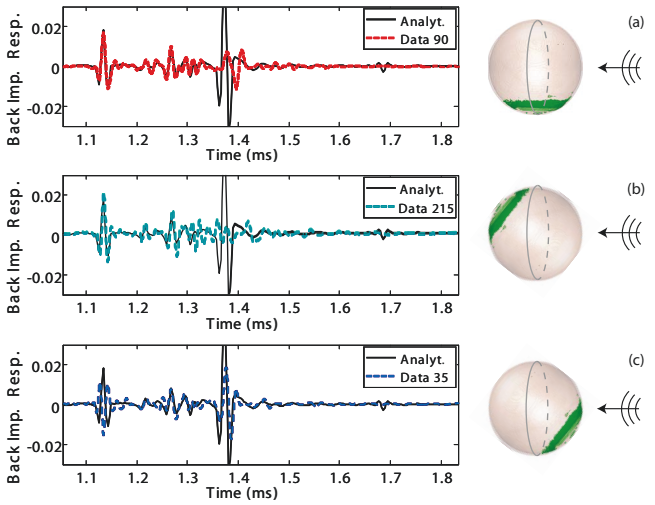

FIG. 18. (Color online) Model–data comparison of backscattering by the resin-filled fiberglass shell (impulse response). The analytical model is applied. On the left-hand side, the impulse response is shown as the insonification aspect varies; on the right-hand side, the cartoons show the position of the annular air pocket at the different aspects of insonification: response at (a) 35°, (b) 90°, and (c) 215°.

hemisphere where the CT scan localized the air pocket. Figure 16 compares the time envelope of the signal in the presence and absence of the air interlayer below the shell wall. A strong echo is reflected back from the internal interface of the shell wall only if there is air at the other side; otherwise the impedance between the shell and filler materials is too low to give a significant reflection at the interface. Measurements were performed on a grid of points having an approximate resolution of 5 mm [see Fig. 17(a)]. The 3D map of points where the internal air was detected is shown in Fig. 17(b). Detection is decided by thresholding the measured signal in the time window between 0.0512 and 0.053 ms. The cross labeled with P on the map indicates the pole of the sphere and corresponds to the pole on the symmetry axis drawn on the CT-scan image of Fig. 14.

B. Model–data comparison and discussion

Based on the results of the NDT measurements, it is possible to discuss the acoustic measurements of the fiberglass-coated resin sphere and their comparison to the simulation obtained by feeding an ideal analytical model (assuming perfect bonded contact at the filler–shell interface) with the material parameters estimated in Sec. IV (see Fig. 18). The parameters still appear to be valid, as confirmed by the generally satisfactory agreement in amplitude and phase of both the longitudinal and transverse Whispering–Gallery wave echoes. The amplitude and dispersion of the Scholte–

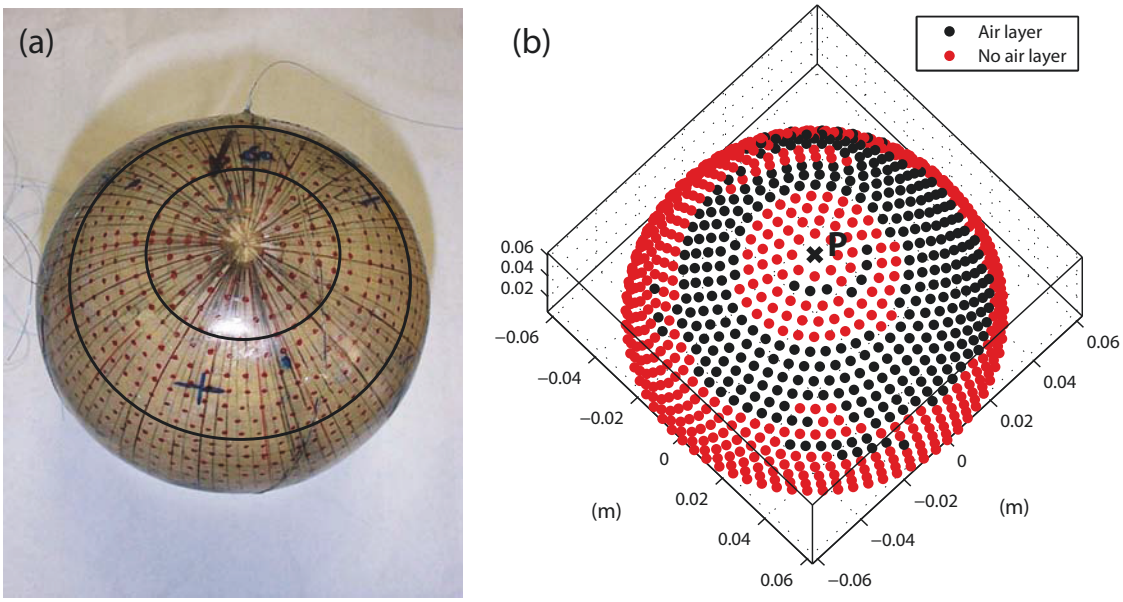

FIG. 17. (Color online) Ultrasound measurement of the resin-filled shell. (a) The hemisphere containing the internal flaw. The grid of dots indicates the points of ultrasound measurement. The two black circles delimit the area of the air pocket as detected by the ultrasonic measurements (b). At the top of (a) the thin wire used for suspension can be distinguished. (b) Three-dimensional mapping of the measured points on the sphere surface, where the detection of internal air is localized.

Stoneley wave echo strongly depends on the air-pocket location with respect to the travel path of the wave itself. As the wave is subsonic, its generating line is the circumference drawn on the sphere in the right column of Fig. 18. The first echo of the wave reradiates back from the sphere at the same circumferential line after the wave has traveled along the shell–filler interface around the nonilluminated hemisphere. Hence, the Scholte–Stoneley wave echo amplitude and shape deviate from the analytical prediction for the ideal geometry depending on the insonification angle, i.e., depending on the degree of interaction with the air pocket. When the air layer is completely included in the nonilluminated hemisphere and, hence, its interaction with the wave is total [Fig. 18(b)], the wave echo almost disappears; when half of the area of the air pocket interacts with the wave [Fig. 18(a)], the wave echo is significantly attenuated and dispersed. Finally, Fig. 18(c) shows a situation in which the interaction is very limited, and, hence, the phase of the Scholte–Stoneley wave is in good agreement with the ideal expectations, while its amplitude is lower than expected, but much higher than in the other measurements.

Due to the asymmetry of the sphere interior, attempts to apply analytical models with different hypotheses of boundary conditions at the filler–shell interface (such as pure transverse slip,[29] or discontinuity of one or both displacement components[31]) are unsuccessful in properly modeling the Scholte–Stoneley wave echo since they apply the same boundary condition at any point of the interface. Only a fully 3D model can provide high-fidelity solutions to this problem, but it would need an extremely precise knowledge of the size and distribution of all the main inhomogeneities (air pockets) and of the actual type of local contact at the interface, which is hard to measure or estimate, and, hence, is not a practical approach.

However, the roughly axisymmetric shape of this air pocket makes it possible to apply the modeling tool AXISCAT[17] with the purpose to refine the model–data comparison achievable by analytical tools. AXISCAT is a frequency-domain finite-element model for scattering by axially symmetric, fluid-loaded structures subject to a nonsymmetric forcing.

The geometry of the air pocket is modeled from the NDT measurements as described in the following (see Fig. 19). An equivalent, average width and thickness of the ring is estimated around the axis of symmetry of the sphere, and used to model an axisymmetric air pocket. The mesh is discretized with triangular cubic Lagrange elements of maximum edge length equal to 1.7 mm. Around the corners of the air pocket the mesh is refined with element clouds having edge lengths on the order of 0.1 mm. The result of the model–data comparison, obtained by feeding the model with the material parameters inverted in Sec. IV, is shown in Fig. 20, where the data at 90° of aspect are selected. In the time domain, the agreement for the Scholte–Stoneley wave echo has much improved with respect to the analytical model result in terms of both amplitude and initial phase, while the dispersion of the echo cannot be perfectly modeled. The remaining dispersion mismatch is particularly evident in the frequency domain, where the pattern of peaks/dips characterizing the target strength is very sensitive to the interaction between the specular and the Scholte–Stoneley echoes. This mismatch may be due either to a not sufficiently accurate modeling of the geometry of the air pocket, or to the total absence in the model of other significantly big air bubbles (e.g., those ones close to the sphere pole as shown in Fig. 15), but also from the presence of boundary conditions at the filler–shell interface locally or generally different from the perfect-contact condition assumed in the model. As mentioned earlier, precise knowledge of local contact conditions is hard to obtain, as they can vary point to point and from object to object, depending on a series of factors, including the external temperature during manufacturing, which could not be precisely controlled. The very good agreement in the

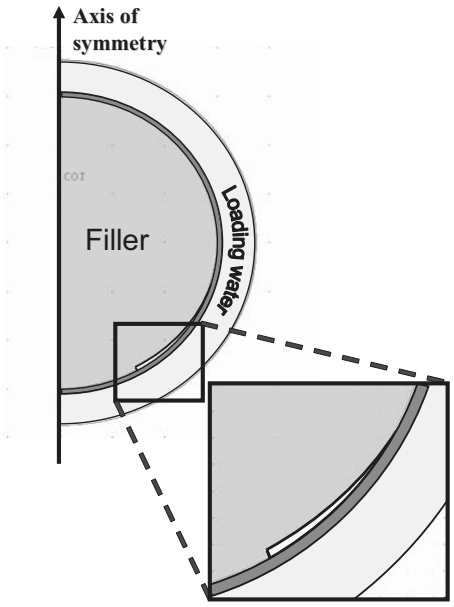

FIG. 19. Model of the resin-filled shell in AXISCAT: An axially symmetric three-dimensional object is obtained by rotation of the two-dimensional surface around the symmetry axis. The geometry of the air-pocket cross section is shown in the blow-up.

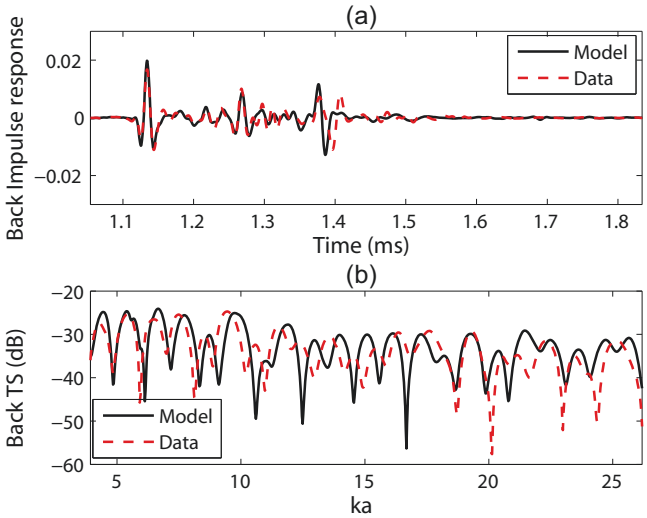

FIG. 20. (Color online) Model–data comparison of backscattering by the resin-filled fiberglass shell: (a) Time impulse response and (b) target strength. The simulation is obtained from AXISCAT. The data are acquired at the insonification angle of 90°.

times of arrival of the Whispering–Gallery waves between model and data suggests not only that the material parameters used are correct, but also that the filler material is acoustically nondispersive in the bandwidth, and, hence, that the heterogeneities noticed in the CT scan are acoustically transparent at these frequencies. As predicted by theory, the fiberglass shell appears practically transparent.

The results of comparison between the model and the data at the other insonification aspects are not reported here. At the nominal aspect angles of 35° and 215°, the agreement is similar, but worse than the result obtained at 90°. The uncertainty in the orientation of the air pocket with respect to the direction of insonification is higher. Furthermore, in these geometries, the role played by the asymmetric parts of the annular air pocket, which cannot be modeled by AXISCAT, appears to be more relevant.

VI. CONCLUSIONS

A series of monostatic acoustic scattering measurements were conducted in a tank on an epoxy-resin-filled fiberglass spherical shell and its components (filler sphere and void shell) in the frequency bandwidth 15–100 kHz, corresponding roughly to a *ka* range of 5–26. The data were analyzed in terms of elastic waves supported by the structure, and compared to suitable models. Acoustic inversion was applied to the void fiberglass shell and to the solid resin sphere to estimate the respective material properties. The main advantage of the proposed inversion approach consists in the possibility of inverting all the parameters of interest by means of a single, broadband measurement, due to the curved (in particular, circular) cross section of the target, and to the broadband nature of the measurement itself, which allows the simultaneous excitation of all the elastic waves supported within the bandwidth of interest. Furthermore, no *a priori* information is needed except for a precise (on the order of about five-hundredths of a wavelength) knowledge of the geometry (sphere radius and thickness).

Model–data comparisons show that the investigated fiberglass is nondispersive below $ka=17$, beyond which the decay of the S_0 Lamb-type resonance modes is stronger than expected, which may imply a further leakage due to diffraction by the fibers along the wave travel path. The absence of strong elastic waves prevented possible evaluations of the dispersiveness of the material beyond $ka=17$. The epoxy resin appears to be nondispersive over the whole bandwidth investigated.

The main NDT result obtained was that an extended air pocket could be detected in the resin-filled shell by comparing underwater acoustic measurements at various aspects. The flaw was independently measured by x-ray CT scan and ultrasound measurements of the object. This study also exposes some of the potential pitfalls associated with the manufacturing of simple objects made of composite/plastic materials. Furthermore, the results show how much the low-frequency response of an object can change due to material heterogeneities deriving from manufacturing flaws. Hence, this defect was useful to prove the potential of acoustic elastic scattering analysis for SHM applications in the case of highly lossy, multilayered materials.

ACKNOWLEDGMENTS

The authors are grateful to the NURC engineering staff involved in the tank experiment, in particular to A. Figoli, A. Sapienza, and L. Troiano, for their precious help, and to F. Jensen for the fruitful scientific discussions. Special thanks go to S. Jensen, M.D., and G. Tognini, M.D., both from Carrara Hospital, who kindly provided the CT scan data. G. Canepa helped in the 3D reconstruction of the sphere from the CT-scan images. J. Fawcett, from DRDC-Atlantic, provided the analytical modeling tool. Many thanks go to S. Kargl for providing the root finder for void shells of lossless materials. The spheres were manufactured by TechnoWave.

[1]Y. Bar-Cohen, A. K. Mal, and S.-S. Lih, "NDE of composite materials using ultrasonic oblique insonification," Mater. Eval. **51**, 1285–1296 (1993).
[2]D. E. Chimenti, "Guided waves in plates and their use in materials characterization," Appl. Mech. Rev. **50**, 247–284 (1997).
[3]M. J. S. Lowe and O. Diligent, "Low-frequency reflection characteristics of the s_0 Lamb wave from a rectangular notch in a plate," J. Acoust. Soc. Am. **111**, 64–74 (2002).
[4]M. J. S. Lowe, P. Cawley, J.-K. Kao, and O. Diligent, "The low-frequency reflection characteristics of the fundamental antisymmetric Lamb wave a_0 from a rectangular notch in a plate," J. Acoust. Soc. Am. **112**, 2612–2622 (2002).
[5]J. Rajagopalan, K. Balasubramaniam, and C. V. Krishnamurthy, "A phase reconstruction algorithm for Lamb wave based structural health monitoring of anisotropic multilayered composite plates," J. Acoust. Soc. Am. **119**, 872–878 (2006).
[6]Z. Su, L. Ye, and Y. Lu, "Guided Lamb waves for identification of damage in composite structures: A review," J. Sound Vib. **295**, 753–780 (2006).
[7]W. Sachse and Y.-H. Pao, "On the determination of phase and group velocities of dispersive waves in solids," J. Appl. Phys. **49**, 4320–4327 (1978).
[8]T. W. Taylor and A. H. Nayfeh, "Damping characteristics of thick rectangular laminates," J. Acoust. Soc. Am. **100**, 1561–1570 (1996).
[9]H. J. McSkimin and J. P. Andreatch, "A water immersion technique for measuring attenuation and phase velocity of longitudinal waves in plastics," J. Acoust. Soc. Am. **49**, 713–722 (1971).
[10]M. R. Karim, A. K. Mal, and Y. Bar-Cohen, "Inversion of leaky Lamb wave data by simplex algorithm," J. Acoust. Soc. Am. **88**, 482–491 (1990).
[11]D. Fei, D. E. Chimenti, and S. V. Teles, "Material property estimation in thin plates using focused synthetic-aperture acoustic beams," J. Acoust. Soc. Am. **113**, 2599–2610 (2003).
[12]V. K. Kinra, P. T. Jaminet, C. Zhu, and V. R. Iyer, "Simultaneous measurement of the acoustical properties of a thin-layered medium: The inversion problem," J. Acoust. Soc. Am. **95**, 3059–3074 (1994).
[13]G. C. Gaunaurd, D. Brill, H. Haung, P. W. B. Moore, and H. C. Strifors, "Signal processing of the echo signatures returned by submerged shells insonified by dolphin 'clicks': Active classification," J. Acoust. Soc. Am. **103**, 1547–1557 (1998).
[14]A. Tesei, W. L. J. Fox, A. Maguer, and A. Løvik, "Target parameter estimation using resonance scattering analysis applied to air-filled, cylindrical shells in water," J. Acoust. Soc. Am. **108**, 2891–2900 (2000).
[15]S. D. Holland, S. V. Teles, and D. E. Chimenti, "Air-coupled, focused ultrasonic dispersion spectrum reconstruction in plates," J. Acoust. Soc. Am. **115**, 2866–2872 (2004).
[16]A. Tesei, M. Zampolli, and J. A. Fawcett, "Acoustic scattering from solid-filled spherical shells: Parametric study of elastic effects," in *Proceedings of the Eighth European Conference on Underwater Acoustics*, Carvoeiro, Portugal, 12–15 June 2006, pp. 157–162.
[17]M. Zampolli, A. Tesei, F. B. Jensen, N. Malm, and J. B. Blottman, "A computationally efficient finite element model with perfectly matched layers applied to scattering from axially symmetric objects," J. Acoust. Soc.

Am. **122**, 1472–1485 (2007).
[18]N. D. Veksler, *Resonance Acoustic Spectroscopy* (Springer, Berlin, 1993).
[19]S. G. Kargl and P. L. Marston, "Observations and modeling of the backscattering of short tone bursts from a spherical shell: Lamb wave echoes, glory, and axial reverberations," J. Acoust. Soc. Am. **85**, 1014–1028 (1989).
[20]P. L. Marston, "GTD for backscattering from elastic spheres and cylinders in water and the coupling of surface elastic waves with the acoustic field," J. Acoust. Soc. Am. **83**, 25–37 (1988).
[21]K. L. Williams and P. L. Marston, "Backscattering from an elastic sphere: Sommerfeld-Watson transformation and experimental confirmation," J. Acoust. Soc. Am. **78**, 1093–1102 (1985).
[22]B. T. Hefner and P. L. Marston, "Backscattering enhancements associated with subsonic Rayleigh waves on polymer spheres in water: Observation and modeling for acrylic spheres," J. Acoust. Soc. Am. **107**, 1930–1936 (2000).
[23]F. Padilla, M. de Billy, and G. Quentin, "Theoretical and experimental studies of surface waves on solid-fluid interfaces when the value of the fluid sound velocity is located between the shear and the longitudinal ones in the solid," J. Acoust. Soc. Am. **106**, 666–673 (1999).
[24]F. Chati, F. Leon, and G. Maze, "The generation, propagation, and detection of Lamb waves in plates using air-coupled ultrasonic transducers," Acoust. Lett. **24**, 1–4 (1996).
[25]G. S. Sammelmann, D. H. Trivett, and R. H. Hackman, "The acoustic scattering by a submerged, spherical. I. The bifurcation of the dispersion curve for the spherical antisymmetric Lamb wave," J. Acoust. Soc. Am. **85**, 114–124 (1989).
[26]A. Tesei, A. Maguer, W. L. J. Fox, R. Lim, and H. Schmidt, "Measurements and modeling of acoustic scattering from partially and completely buried spherical shells," J. Acoust. Soc. Am. **112**, 1817–1830 (2002).
[27]A. D. Pierce, *Acoustics. An Introduction to its Physical Principles and Applications* (Acoustical Society of America, New York, 1989).
[28]C. Matteï, X. Jia, and G. Quentin, "Direct experimental investigations of acoustic modes guided by a solid-solid interface using optical interferometry," J. Acoust. Soc. Am. **102**, 1532–1539 (1997).
[29]G. J. Kühn and A. Lutsch, "Elastic wave mode conversion at a solid-solid boundary with transverse slip," J. Acoust. Soc. Am. **33**, 949–954 (1961).
[30]G. S. Murty, "A theoretical model for the attenuation and dispersion of Stoneley waves at the loosely bonded interface of elastic half spaces," Phys. Earth Planet. Inter. **11**, 65–79 (1975).
[31]S. I. Rokhlin and Y. Wang, "Analysis of boundary conditions for elastic wave interaction with an interface between two solids," J. Acoust. Soc. Am. **89**, 503–515 (1991).
[32]I. A. Viktorov, *Rayleigh and Lamb Waves. Physical Theory and Applications* (Plenum, New York, 1967).
[33]S. I. Rokhlin, D. K. Lewis, K. F. Graff, and L. Adler, "Real-time study of frequency dependence of attenuation and velocity of ultrasonic waves during the curing reaction of epoxy resin," J. Acoust. Soc. Am. **79**, 1786–1793 (1986).

Document Data Sheet

Security Classification		Project No.
Document Serial No. NURC-PR-2008-007	Date of Issue September 2008	Total Pages 14 pp.

Author(s)

Tesei, A., Guerrini, P., Zampolli, M.

Title

Tank measurements of scattering from a resin-filled fibreglass spherical shell with internal flaws.

Abstract

Keywords

Issuing Organization

NURC
Viale San Bartolomeo 400, 19126 La Spezia, Italy

[From N. America:
NURC
(New York) APO AE 09613-5000]

Tel: +39 0187 527 361
Fax:+39 0187 527 700

E-mail: library@nurc.nato.int